Rapid restoration of electric vehicle battery performance while driving at cold temperatures

Guangsheng Zhang[a], Shanhai Ge[b], Xiao-Guang Yang[a], Yongjun Leng[a], Dan Marple[a], Chao-Yang Wang[a],*

[a] Department of Mechanical and Nuclear Engineering and Electrochemical Engine Center (ECEC), The Pennsylvania State University, University Park, PA 16802, USA
[b] EC Power, 341 Science Park Road, State College, PA 16803, USA

HIGHLIGHTS

- A control strategy that rapidly restores EV battery power while driving in cold.
- It also enables full recovery of regenerative braking energy.
- It could increase EV cruise range in cold, e.g. 49% at −40 °C in US06 drive cycle.

GRAPHICAL ABSTRACT
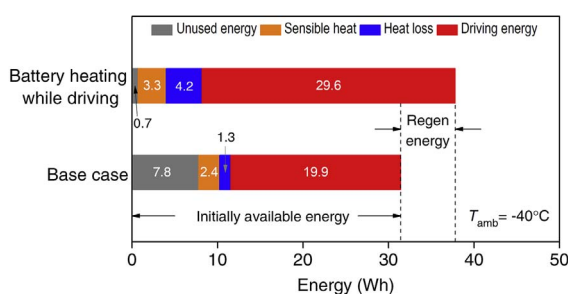
ABSTRACT

Electric vehicles (EVs) driven in cold weather experience two major drawbacks of Li-ion batteries: drastic power loss (up to 10-fold at −30 °C) and restriction of regenerative braking at temperatures below 5–10 °C. Both factors greatly reduce cruise range, exacerbating drivers' range anxiety in winter. While preheating the battery before driving is a practice widely adopted to maintain battery power and EV drivability, it is time-consuming (on the order of 40 min) and prohibits instantaneous mobility. Here we reveal a control strategy that can rapidly restore EV battery power and permit full regeneration while driving at temperatures as low as −40 °C. The strategy involves heating the battery internally during regenerative braking and rest periods of driving. We show that this technique fully restores room-temperature battery power and regeneration in 13, 33, 46, 56 and 112 s into uninterrupted driving in 0, −10, −20, −30 and −40 °C environments, respectively. Correspondingly, the strategy significantly increases cruise range of a vehicle operated at cold temperatures, e.g. 49% at −40 °C in simulated US06 driving cycle tests. The present work suggests that smart batteries with embedded sensing/actuation can leapfrog in performance.

1. Introduction

Drastically reduced driving range [1–4] is a major challenge for electric vehicles (EVs) operating at subzero temperatures as it exacerbate drivers' range anxiety [5]. Two technical problems of Li-ion batteries are particularly long-standing. First, regenerative braking is restricted or completely turned off at cold temperatures due to the phenomena of lithium plating that could severely reduce battery life and increase safety hazards [6,7]. Second, there is significant power loss, up to 10 fold at −30 °C [8], due to sluggish reaction kinetics, slow diffusion, reduced electrolyte conductivity, and increased solid-electrolyte interface (SEI) resistance at low temperatures [9–13]. Great

---

efforts have been made to increase battery power at cold temperatures, notably reformulating electrolytes [14–18], hybridizing batteries with high-power supercapacitors [19], and preheating batteries before driving [20–27]. Among these approaches, battery preheating has been extensively investigated [22–27] due to its relatively simple implementation. But preheating is slow, typically tens of minutes [23–25], and inconvenient, prohibiting instantaneous mobility of EVs. Here we demonstrate an active control strategy that can rapidly restore EV battery power while driving, which eliminates any need to wait for preheating. This control strategy represents a new paradigm allowing batteries to be actively controlled and manipulated. We also demonstrate, through simulated US06 driving cycle tests and an energy balance analysis, that power restoration while driving could significantly increase EV driving range by fully recuperating braking energy and significantly increasing utilization of energy stored.

2. Experimental

2.1. Experimental system

Self-heating Li-ion battery (SHLB) cells with two embedded nickel foils, schematically shown in Fig. 1c and same as that reported earlier [28], are used as experimental cells. Each cell has a 152 × 75 mm footprint area, has nominal capacity of 9.5 Ah and weighs 210 g. Two pieces of polyethylene terephthalate coated nickel foil, each with resistance of 78 milli-Ohm at 20 °C, are stacked at ¼ and ¾ of cell thickness for uniform heating. The two pieces of nickel foil are connected in parallel with their total resistance of 39 milli-Ohm at 20 °C. The added weight and cost due to nickel foils are about 1.5% and 0.4% of the baseline battery [8]. $LiNi_{0.6}Co_{0.2}Mn_{0.2}O_2$ and graphite are used as cathode and anode active materials, respectively. More details about SHLB cell fabrication and materials can be found in our previous work [28]. One end of the nickel foils are connected to the negative terminal of SHLB cell while the other end extends out of the cell as an activation terminal (ACT). A switch is placed between positive terminal and ACT terminal. When the switch is ON, the SHLB cell works at heating mode as high current passes through the nickel foils and generates heat very rapidly [28]. When the switch is OFF, the SHLB cell works at normal mode just like a conventional cell without embedded nickel foils. In this study, the switch will be controlled according to EV load profile using a simple yet novel strategy. More details about the control strategy are in section 3.1. If the switch is constantly OFF, the SHLB cell works as a baseline cell.

A T-type thermocouple (SA1-T, OMEGA Engineering) is placed at the center of cell outer surface for monitoring cell surface temperature. A battery tester (BT2000, Arbin) is used to control power output of experimental cell according to profile of US06 driving cycle test, which is derived proportionally from the power profile developed by Keil et al. [19] for 3.3 Ah Li-ion cells. The battery tester is also used to measure external voltage and external current. A relay (EV200, TE Connectivity) is used to work as the switch between positive terminal and activation terminal of the SHLB cell. It is controlled by the battery tester so that it closes only during regen and rest periods of US06 driving cycle. When the cell reaches a desired temperature, 10 °C in this study, the relay is powered off and kept open. A shunt resistor (SHT1-500C075DE, Ohmite) is connected between positive terminal and activation terminal to measure cell current during self-heating. An environmental chamber (Tenney SPX, Thermal Product Solutions) is used to control the ambient temperature. The experimental cell is placed in a home-made thermal insulation box inside the environmental chamber to simulate cooling conditions in EV applications. A data acquisition unit (USB-2408, Measurement Computing Corporation) is used to record cell temperature, current and voltage at 5 Hz during US06 driving cycle tests.

2.2. Test protocol

For all low temperature tests in this study, the protocol is as follows: (1) Fully charging cell at 20 °C (1C, 4.2 V, C/20 cutoff); (2) Cooling cell to desired temperature for at least 6 h to ensure thermal equilibrium; (3) US06 driving cycle testing with first self-heating at the beginning and second self-heating after 5 cycles (50 min into testing), with cutoff voltage at 2.7 V; (4) Warming up cell to 20 °C; (5) Further continue US06 driving cycle test at 20 °C. Note that step (1) provides information on initially available energy; step (3) provides information on the regenerative breaking energy and driving energy; and step (5) provides information on unused energy.

3. Results and discussion

3.1. Control strategy of "battery heating while driving"

Fig. 1a shows the measured internal resistance of a 9.5 Ah Li-ion pouch cell during 1C discharge at different temperatures. As can be seen, the cell resistance increases exponentially as temperature decreases. The resistance at −40 °C is about 30 times higher than that at room temperature, indicating proportional power loss. Fig. 1b schematically depicts the load profile scaled for a 9.5 Ah Li-ion cell during a US06 driving cycle test as adapted from that of Keil et al. [19]. Three regimes can be observed from the profile: battery discharge for vehicle driving (power is negative), regenerative braking (power is positive) and rest (power is zero). Energy from the regenerative braking, which is up to 22% of energy for driving in the US06 profile, can be used to charge the battery for later use if the battery is warm enough. But if the battery is too cold, regenerative braking must be much restricted or completely turned off to avoid lithium plating, wasting a significant amount of energy. To fully recuperate this braking energy without lithium plating and restore battery power at low temperatures, we propose a new active control strategy, named "Battery Heating While Driving", where braking energy is used for internal heating. Once the battery is sufficiently warmed, the braking energy is subsequently used to charge battery active materials. This control strategy not only enables full recovery of braking energy, but also rapidly restores battery power performance without interrupting vehicle functionality and mobility.

The active control strategy is implemented on a recently discovered self-heating Li-ion battery (SHLB) [8,28]. As schematically shown in Fig. 1c, a SHLB cell has a nickel foil embedded for highly efficient and rapid self-heating [28]. One end of the foil is connected to the negative terminal while the other end extends out of the cell as an activation terminal (ACT). A switch is placed between positive terminal and ACT terminal. During regenerative braking (indicated by positive value of external current) and when the battery is cold (indicated by $T_{cell} < T_{critical}$), the switch is turned ON. External current from regenerative braking is thus diverted to the nickel foil for heating the battery, instead of being wasted on charging the battery materials which could cause lithium plating. Simultaneously the battery may discharge the current through the nickel foil to augment rate of battery heating and power restoration. When the vehicle needs power for acceleration or driving (indicated by negative value of external current), or the battery is already warm enough (indicated by $T_{cell} \geq T_{critical}$), the switch is turned OFF so that the SHLB functions just like a conventional two-terminal battery. To accelerate battery heating and power restoration, the switch may also be turned ON during rest periods.

Experimental results of executing the "Battery Heating While Driving" control strategy in a simulated US06 driving cycle test at −40 °C are shown in Fig. 1(d)–(g). It can be seen from Fig. 1d that not only is the cell discharge current (blue) equal to the external current (black) during driving periods to provide traction power, but also the cell undergoes high-rate discharge during rest and regen periods (hatched area) for rapid self-heating. Note that cell current automatically
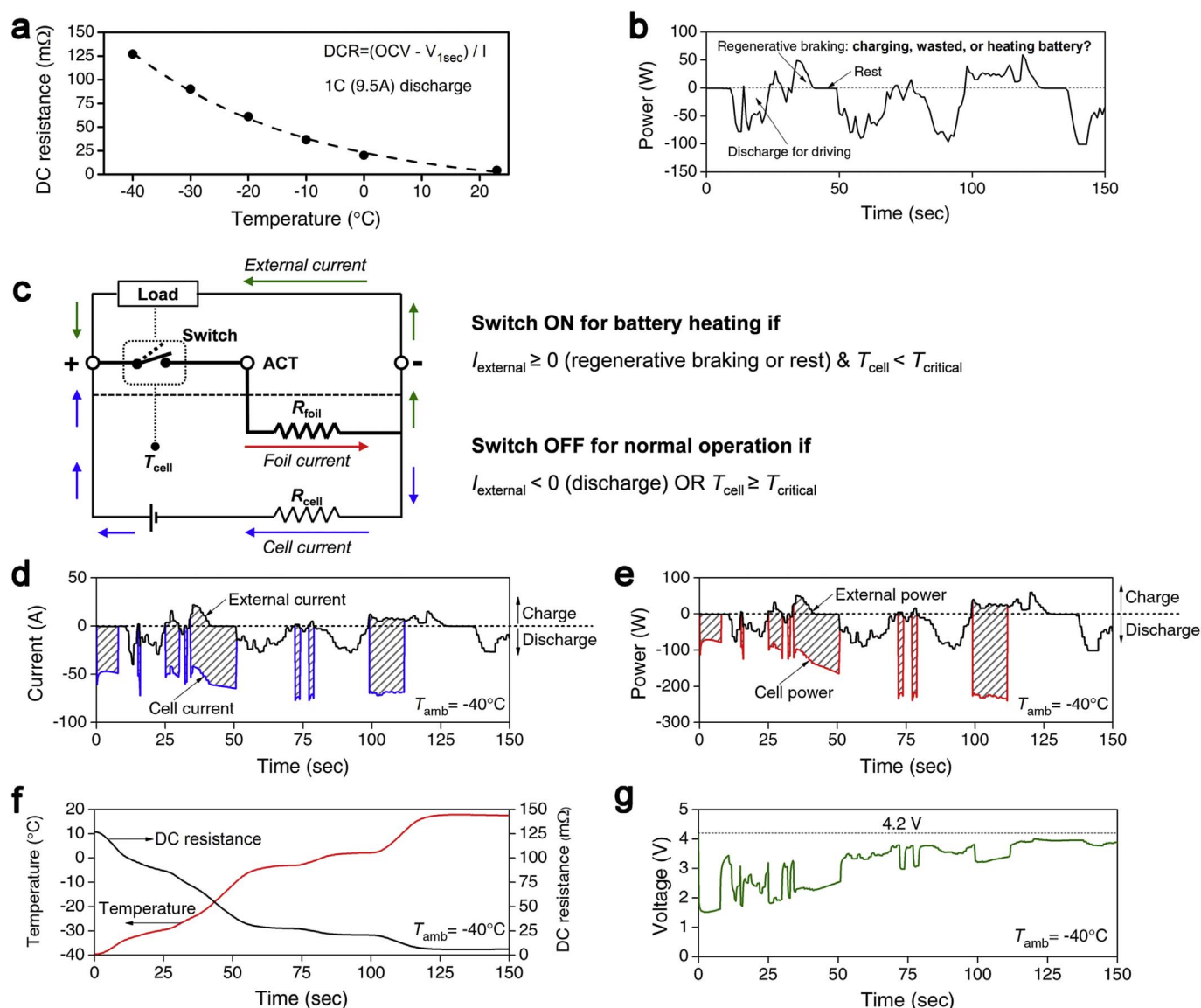
Fig. 1. Control strategy of "Battery Heating While Driving". (a) Exponential increase of the Li-ion battery internal resistance with lower temperatures. (b) Power profile during a simulated US06 driving cycle test. (c) Working principle and schematic of power restoration while driving with a self-heating Li-ion battery. (d) Measured external current and cell current during power restoration while driving in simulated US06 driving cycle test at −40 °C. (e) Measured external power and cell power. (f) Measured cell temperature and estimated internal resistance. (g) Measured cell voltage.

changes with external current during rest and region period, leading to nearly constant total current flowing through the nickel foil. As shown in Fig. 1e, the results of external power and cell power exhibit a trend very similar to that of currents. External power nicely follows the US06 driving cycle load profile in Fig. 1b, confirming that the active control strategy does not interrupt any vehicle functionality or mobility. With the hatched area representing energy used for battery heating, it is obvious that braking energy is fully recovered, initially for battery heating and then for battery charging. As the battery cell is heated, its temperature rapidly increases, as can be seen in Fig. 1f, from −40 °C to 10 °C (chosen to be $T_{critical}$) in 112 s. Correspondingly, its internal resistance (estimated from the relation shown in Fig. 1a) rapidly decreases from over 125 mΩ to about 10 mΩ, which signifies completion of power restoration. Cell temperature further increases to nearly 20 °C due to lag of surface temperature measured.

Similar results at other cold temperatures (0, −10, −20, and −30 °C) are presented in Fig.S1-S4 in the Supplementary Materials. As can be seen, it takes 13, 33, 46, and 56 s for the SHLB cell to reach 10 °C from low temperatures of 0, −10, −20, and −30 °C, respectively. To

our best knowledge, this is the first demonstration showing that battery heating and power restoration while driving can be so quick, without any interruption of vehicle functionality and mobility. As revealed in our previous work [28], such quick heating can be attributed to significantly enhanced heat generation by the nickel foil embedded in SHLB cell. Using similar analysis, and based on measured cell temperatures in this study, it can be estimated that nickel foil contributes 66%, 59%, 55%, 46% and 43% of total heat generation for the self-heating process at 0, −10, −20, −30 and −40 °C.

It is worth noting that the rapid self-heating process has little effects on battery durability. As demonstrated in our previous work [8], SHLB cell showed only 7.2% capacity degradation after 500 times of rapid self-heating from −30 °C. With the improved design of incorporating two sheets of nickel foil that significantly reduces the temperature gradient inside SHLB cell [28,29], the effects of self-heating on durability would be even smaller.
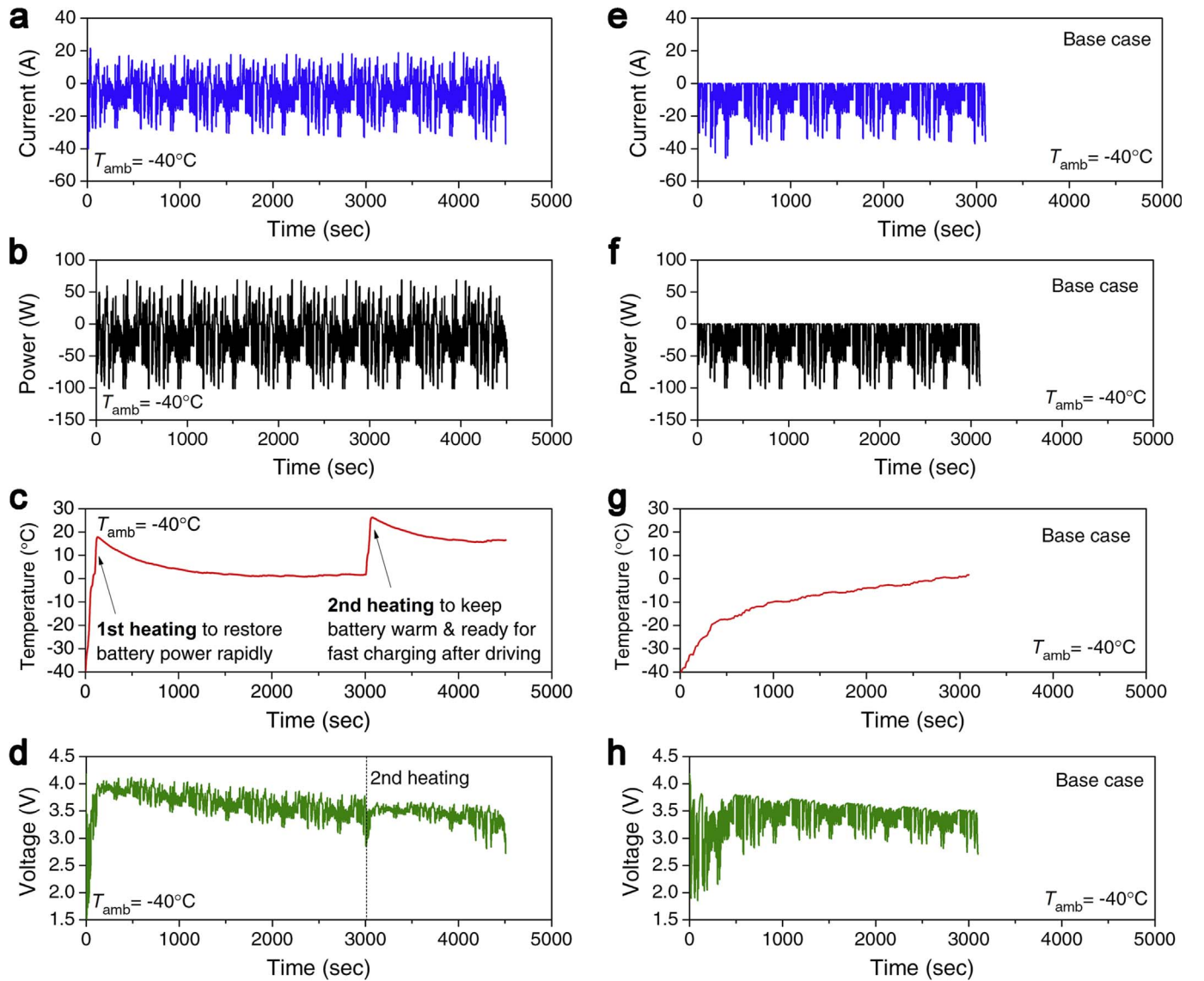
Fig. 2. Comparison between the "Battery Heating While Driving" case and the base case during US06 driving cycle test at −40 °C.

3.2. Comparison between the "battery heating while driving" case with the base case

After rapid initial power restoration, the SHLB cell continues to be tested according to US06 driving power profile. Each US06 drive cycle takes 600 s and the test is repeated until cell voltage reaches cutoff voltage of 2.7 V. The results of external power, current, cell temperature and cell voltage during such a full test at −40 °C are shown in Fig. 2(a)–(d). Note that −40 °C was chosen as it represents the coldest operating environment for electric vehicles set by U.S. Department of Energy [30]. For comparison, the results of the base case without the strategy of battery heating while driving are shown in Fig. 2(e)–(h). By comparing the case of power restoration while driving with the base case, it is obvious that the presented control strategy heats up the battery much faster than the base case. It takes only 112 s to heat the battery to almost 20 °C, which subsequently enables full recovery of braking energy, while in the base case the cell temperature reaches slightly above 0 °C after more than 3000 s of driving, prohibiting recovery of braking energy during most of the driving profile. Notice that a second rapid heating process is activated after five US06 cycles when the temperature of the experimental cell drops below 2 °C due to heat loss to the environmental chamber. In practice, a second heating could

be applied based on battery thermal insulation conditions and vehicle driving conditions. The second heating keeps the battery warm enough until the end of testing, which not only enables full regeneration of braking energy but also increases utilization of stored energy. As expected, SHLB cell with the control strategy operates 46% longer in time, with 49% more energy used for driving, than the base case.

3.3. Energy balance analysis

To further understand the mechanisms underlying battery power restoration at low temperatures, an energy balance analysis is carried out. Energy balance during a driving cycle can be generally written as:

$$E_{available} + E_{regen} = E_{drive} + E_{sensible\ heat} + E_{heat\ loss} + E_{unused} \qquad (1)$$

In the equation $E_{available}$ is the initially available electric energy stored in a fully charged cell, E_{regen} represents the electric energy regenerated from vehicle braking, E_{drive} is the electric energy used for driving, $E_{sensible\ heat}$ is the heat absorbed by cell materials as its temperature rises during test, $E_{heat\ loss}$ is the heat loss to the low-temperature surroundings, and E_{unused} is the electric energy remaining in the cell when the driving cycle ends, e.g. after V < V$_{cut-off}$.

Values of E_{regen} and E_{drive} are directly measured by integrating the

discharge and charge energy of a driving power cycle, respectively. E_{unused} is usually negligible for driving profiles at 20 °C. $E_{sensible\ heat}$ can be estimated from specific heat capacity (c_p, typically 1000 J/kg· °C or 0.278 Wh/kg· °C), cell mass ($m = 0.21$ kg in this study) and measured cell temperature rise ($T_{cell,\ f} - T_{cell,\ i}$) by:

$$E_{\text{sensible heat}} = c_p m (T_{cell,f} - T_{cell,i}) \qquad (2)$$

$E_{heat\ loss}$ is related to thermal insulation by:

$$E_{\text{heat loss}} = A \int_0^\tau h(T_{cell} - T_{amb})dt \qquad (3)$$

in which h is the overall heat transfer coefficient and A is the heat transfer surface area (~ 0.023 m²). During a US06 driving cycle at 20 °C, $E_{sensible\ heat}$ and $E_{heat\ loss}$ are negligibly small as compared to E_{regen} and E_{drive}. Consequently, $E_{available}$, physically proportional to the specific energy density, ρ_e, measured at C/3 rate, is found from Eq. (1) to be 31.4 Wh, i.e. $E_{available} = \alpha m \rho_e$ where $\alpha = 0.9$ due to the average discharge rate in the US06 profile being higher than C/3 used in defining the specific energy density, ρ_e.

Finally, the regen energy, E_{regen}, is usually proportional to E_{drive}, i.e. $E_{regen} = \beta E_{drive}$ where $\beta = 0.22$ for the US 06 driving cycle if regeneration is fully activated. To summarize the above, Equation (1) can be rewritten as:

$$\alpha m \rho_e + \beta E_{drive} = E_{drive} + c_p m (T_{cell,f} - T_{cell,i}) + A \int_0^\tau h(T_{cell} - T_{amb})dt$$
$$+ E_{unused} \qquad (4)$$

When Eq. (4) is applied to driving experiments at low temperatures, E_{drive} can be simply measured from the total discharge energy, and E_{unused} is determined by taking a tested battery to 20 °C and further disharging the residual energy at 20 °C. With all other values known, Eq. (1) is left with only one unknown, h, the overall heat transfer coefficient for heat loss. Thus-determined h is found to be 2.8 ± 0.3 W/m²· °C over the temperature range of −40 to 20 °C.

The results of energy breakdown analysis per Eq. (1) are shown in Fig. 3 for US06 tests at −40 °C. It can be seen that driving energy is significantly increased with the present control strategy, 49% more than that in the base case, despite that some stored energy is used for self-heating at the beginning. Such significant increase comes from two sources. One is that the unused energy is much less, more than 10 times less, than that in the base case due to much increased cell temperature at the end of the driving test. The other is that energy from regenerative braking, about 22% of total energy for driving, is fully activated.

3.4. Driving energy at different temperatures

The results of measured driving energy at different temperatures are plotted as symbols in Fig. 4. We note that the "Battery Heating While Driving" strategy delivered 78, 80, 85 and 90% of the room-
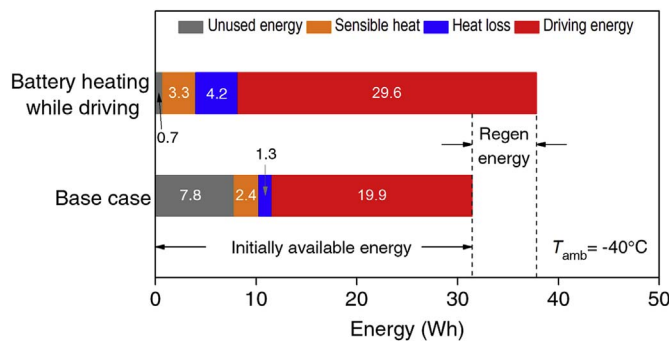

Fig. 3. Comparison of energy balance between the "Battery Heating While Driving" case and the base case during simulated US06 drive cycle tests at −40 °C.
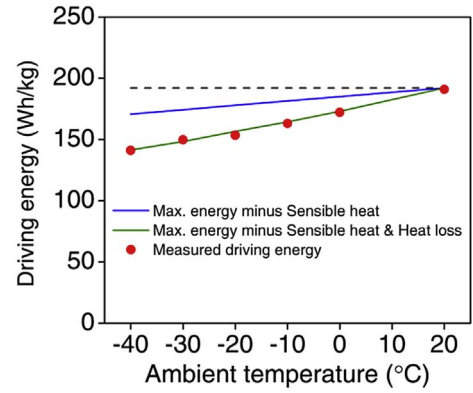

Fig. 4. Driving energy after rapid power restoration at different temperatures. (Black dashed line shows room-temperature driving energy.)

temperature driving energy at −30, −20, −10 and 0 °C, respectively.

For comparison, we also plot three theoretical curves: (1) the room-temperature driving energy, (2) that minus the sensible heat absorbed by battery materials when the cell temperature rises from the initial ambient temperature to 20 °C, and (3) that further minus the heat loss from the battery pack to the cold surroundings. For driving below room temperature, i.e. 20 °C, the last three terms on the right hand side of Eq. (4) become negligible so that the room-temperature driving energy is simply given by:

$$\frac{E_{\text{drive}}}{m} = \frac{\alpha \rho_e}{1 - \beta} \qquad (5)$$

Eq. (5) is shown as the black dashed line in Fig. 4.

If only sensible heat is substracted from the maximum energy given by Eq. (5), one has:

$$\frac{E_{\text{drive}}}{m} = \frac{\alpha \rho_e - c_p(T_{cell} - T_{amb})}{1 - \beta} \qquad (6)$$

which gives the blue line in Fig. 4.

If both sensible heat and heat loss are substracted from the maximum energy given by Eq. (5), then one has:

$$\frac{E_{\text{drive}}}{m} = \frac{\alpha \rho_e - c_p(T_{cell} - T_{amb}) - \left(\frac{A}{m}\right) \int_0^\tau h(T_{cell} - T_{amb})dt}{1 - \beta} \qquad (7)$$

giving rise to the green line in Fig. 4. Note that in Eqs. (5)–(7), $\alpha = 0.9$, $\beta = 0.22$ and h = 2.8 W/m²· °C. To generate blue and green lines, we set T_{cell} in Eqs. (6) and (7) at 20 °C for simplicity, while the actual cell temperature varies below 20 °C as can be seen from Fig. 2c. Thus, blue and green lines might have been over-estimated.

By comparing the green line and the red symbols in Fig. 4, it can be seen that actual measured driving energy from the SHLB cell is already close to the theoretical maximum energy after subtracting sensible heat absorbed by the battery and heat loss to the surroundings, suggesting high effectiveness of the present control strategy in maximizing driving energy.

3.5. Projection of driving energy for future energy dense Li-ion cells

It is worth noting that the present control strategy would also work for future batteries of higher energy density. The benefits would be even more significant because inevitable sensible heat and heat loss would be relatively less with more energy dense batteries. Fig. 5 shows a projection of the driving energy for a future energy-dense Li-ion cell (300 Wh/kg), assuming similar thermal-insulation conditions and similar driving protocol to this study, i.e. using Eqs. (5)–(7). Comparison between Figs. 4 and 5 shows that sensible heat, which reflects energy absorbed by battery materials upon heating, would become much less for energy-dense batteries, decreasing from 8.7% of maximum energy
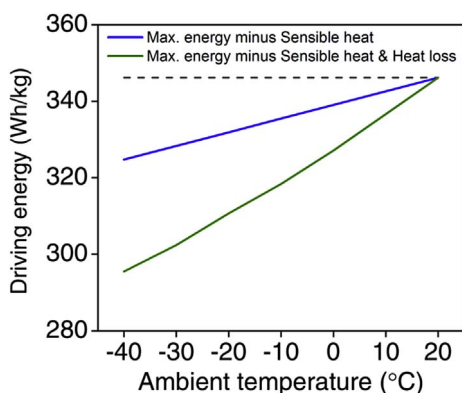
Fig. 5. Projection of driving energy for future energy dense Li-ion cells. (Assuming energy density of 300 Wh/kg, and similar thermal-insulation conditions to this study.)

to 4.8% at −40 °C, due to relatively lower thermal mass contained in a more energy-dense battery. The ratio of heat loss to maximum energy would also drop, from 11.9% to 6.6% for −40 °C environment. As a result, the ratio of driving energy at a low temperature to that at 20 °C would increase, e.g. from 74% to 85% for −40 °C test. This clearly suggests that the present control strategy would be even more effective for future energy-dense batteries. Additionally Fig. 5 implies that the next measure to improve driving energy at low temperatures, i.e. from 85 to 94% at −40 °C, should come from curbing heat loss to the cold surroundings by improving thermal insulation.

4. Conclusions

We have demonstrated, both experimentally and theoretically, a novel control strategy for rapid power restoration of EV batteries while driving at low temperatures. It eliminates any wait for battery pre-heating, thus offering instantaneous availability of vehicles. The control strategy is made possible by a self-heating Li-ion battery and involves activating self-heating during braking and rest periods of initial driving, thereby not compromising battery power delivery to the vehicle. The process of self-heating while driving is found to be very energy-efficient and fast, with the heating energy supplied from both stored battery energy and vehicle braking energy. It enables full recovery of regenerative braking energy and much increased utilization of available energy even at low temperatures, which in turn significantly increases vehicle cruise range by nearly 50% at −40 °C. With the battery temperature remaining high, near room temperature, at the end of driving, the vehicles would also be primed for fast recharging after driving. An energy balance analysis suggests that driving energy at low temperatures could be further increased for future batteries of higher energy density in a large part due to their relative lower thermal mass. We showed that delivering 90% of the room-temperature driving energy in the −40 °C environment is highly possible with a future battery of higher energy density and improved thermal insulation of a battery pack, making functionality and performance of EVs truly weather independent like internal combustion engines. This work paves the way for specification of all-climate range (ACR) (−20 °C to 40 °C), a new criterion intended to measure cruise range of battery electric cars in real-world conditions.

The present control strategy also points to a new paradigm in which active control and manipulation of EV batteries could override passive endurance imposed by severely limited battery electrochemistry for superior operation and energy efficiency of EVs. Further efforts are warranted, e.g. in obtaining quantitative and direct evidence of lithium-plating prevention with SHLB through numerical modeling and post-mortem analysis, validating and analyzing this control strategy across a variety of drive cycles [31] and operating conditions, applying it to battery packs, and developing sophisticated control strategies for more energy optimization.

Appendix A. Supplementary data

Supplementary data related to this article can be found at http://dx.doi.org/10.1016/j.jpowsour.2017.10.029.

References

[1] N. Meyer, I. Whittal, M. Christenson, A. Loiselle-Lapointe, EVS26-International Battery, Hybrid and Fuel Cell Electric Vehicle Symposium, 2012, pp. 1–11.
[2] J. Laurikko, R. Granström, A. Haakana, EVS27-International Battery, Hybrid and Fuel Cell Electric Vehicle Symposium, 2013, pp. 1–12.
[3] K. Stutenberg, 2014 U.S. DOE Vehicle Technologies Program Annual Merit Review and Peer Evaluation Meeting, 2014 http://energy.gov/sites/prod/files/2014/07/f17/vss030_stutenberg_2014_o.pdf.
[4] AAA, http://newsroom.aaa.com/2014/03/extreme-temperatures-affect-electric-vehicle-driving-range-aaa-says, (2014).
[5] J. Neubauer, E. Wood, J. Power Sources 257 (2014) 12–20.
[6] T. Waldmann, B.-I. Hogg, M. Kasper, S. Grolleau, C.G. Couceiro, K. Trad, B.P. Matadi, M. Wohlfahrt-Mehrens, J. Electrochem. Soc. 163 (2016) A1232–A1238.
[7] P. Keil, A. Jossen, EVS28-International Electric Vehicle Symposium and Exhibition, 2015, pp. 1–11.
[8] C.Y. Wang, G. Zhang, S. Ge, T. Xu, Y. Ji, X.G. Yang, Y. Leng, Nature 529 (2016) 515–518.
[9] C.K. Huang, J.S. Sakamoto, J. Wolfenstine, S. Surampudi, J. Electrochem. Soc. 147 (2000) 2893–2896.
[10] H.-p. Lin, D. Chua, M. Salomon, H.-C. Shiao, M. Hendrickson, E. Plichta, S. Slane, Electrochem. Solid-State Lett. 4 (2001) A71–A73.
[11] L.O. Valoen, J.N. Reimers, J. Electrochem. Soc. 152 (2005) A882–A891.
[12] K.L. Gering, ECS Trans. 1 (2006) 119–149.
[13] Y. Ji, Y. Zhang, C.Y. Wang, J. Electrochem. Soc. 160 (2013) A636–A649.
[14] Y. Ein-Eli, S.R. Thomas, R. Chadha, T.J. Blakley, V.R. Koch, J. Electrochem. Soc. 144 (1997) 823–829.
[15] S.S. Zhang, K. Xu, T.R. Jow, Electrochem. Commun. 4 (2002) 928–932.
[16] M.C. Smart, B.V. Ratnakumar, L.D. Whitcanack, K.B. Chin, S. Surampudi, H. Croft, D. Tice, R. Staniewicz, J. Power Sources 119–121 (2003) 349–358.
[17] B.K. Mandal, A.K. Padhi, Z. Shi, S. Chakraborty, R. Filler, J. Power Sources 162 (2006) 690–695.
[18] S. Li, X. Li, J. Liu, Z. Shang, X. Cui, Ionics 21 (2015) 901–907.
[19] P. Keil, M. Englberger, A. Jossen, IEEE Trans. Veh. Technol. 65 (2016) 998–1006.
[20] A. Vlahinos, A.A. Pesaran, SAE Technical Paper 2002-01-1975, (2002), pp. 1–8.
[21] T.A. Stuart, A. Hande, J. Power Sources 129 (2004) 368–378.
[22] Y. Ji, C.Y. Wang, Electrochim. Acta 107 (2013) 664–674.
[23] H.-S. Song, J.-B. Jeong, B.-H. Lee, D.-H. Shin, B.-H. Kim, T.-H. Kim, H. Heo, 2012 IEEE Vehicle Power and Propulsion Conference, 2012, pp. 1198–1201.
[24] J. Zhang, H. Ge, Z. Li, Z. Ding, J. Power Sources 273 (2015) 1030–1037.
[25] M. Zuniga, J. Jaguemont, L. Boulon, Y. Dube, 2015 IEEE Vehicle Power and Propulsion Conference (VPPC), 2015, pp. 1–6.
[26] H. Ge, J. Huang, J. Zhang, Z. Li, J. Electrochem. Soc. 163 (2016) A290–A299.
[27] J. Zhu, Z. Sun, X. Wei, H. Dai, Int. J. Energy Res. 40 (2016) 1869–1883.
[28] G. Zhang, S. Ge, T. Xu, X.G. Yang, H. Tian, C.Y. Wang, Electrochim. Acta 218 (2016) 149–155.
[29] X.G. Yang, G. Zhang, C.Y. Wang, J. Power Sources 328 (2016) 203–211.
[30] USABC, Department of Energy (DoE) Final Report Compilation for the Research and Development of High-power and High-energy Electrochemical Storage Devices, (2014) https://www.osti.gov/scitech/servlets/purl/1160224/.
[31] EPA, Dynamometer Drive Schedules, (2017) https://www.epa.gov/vehicle-and-fuel-emissions-testing/dynamometer-drive-schedules.